ELSEVIER

Journal of Nuclear Materials 298 (2001) 297–308

journal of nuclear materials

www.elsevier.com/locate/jnucmat

In situ characterization of Zircaloy-4 oxidation at 500 °C in dry air

J.J. Vermoyal [a,b,*,1], L. Dessemond [a], A. Hammou [a], A. Frichet [b]

[a] *Laboratory of Electrochemistry and Physical-chemistry of Materials and Interfaces, UMR 5631 INPG-CNRS-UJF, 38402 Saint Martin d'Hères, France*

[b] *Framatome Nuclear Fuel, 10 rue Juliette Récamier, 69006 Lyon, France*

Received 7 February 2001; accepted 29 June 2001

Abstract

The in situ oxidation of Zircaloy-4 at 500 °C in dry air was investigated by thermogravimetric analysis (TGA) and electrochemical impedance spectroscopy (EIS). The coating of the alloy by a platinum film as electrode material was observed as not to modify the oxidation kinetic properties. After an initial cubic rate law, a transition to a quasi-linear curve occurs. The independence of the oxidation behavior to the Pt coupling is compatible with oxygen diffusion as the rate-determining step. During the pre-transition step, the rest potential of the cell Pt/oxide/Zy-4, the color of the oxide and the modulus of the single EIS signature indicate the high non-stoichiometry of the oxide. The kinetic transition was proposed to be correlated to the degradation of the film into a partially porous layer. This alteration of the oxide is associated to the appearance of a 1.2 V constant rest potential and the modification of the impedance diagrams in two high modulus contributions. The Cole–Cole representation has been used to demonstrate that the time variation of impedance spectra is related to the oxide growth. An equivalent circuit including two RC loops in series, whose capacitances are frequency dispersed, was proposed to be related to the film structure. Fitted data show that the thickness of the assumed protective layer of the film, close to the metal–oxide interface, is time independent in agreement with a constant oxidation rate. Finally, electrical properties of this inner layer were found to be quite different in pre- and post-transition stage.

1. Introduction

The thermal oxidation of zirconium alloys is generally described by an initial cubic or parabolic pre-transition stage followed by a quasi-linear variation law [1,2]. The oxidation kinetics has been extensively studied under several oxidation conditions (temperature, steam, dry air and oxygen, etc.) in order to elucidate the mechanism of oxide growth and breakdown [3]. Even under similar experimental conditions, the comparison of results shows discrepancies concerning the rate law (cubic or parabolic) better describing the first step of the kinetics [4]. The reaction mechanism was shown to depend on the chemical composition of the material [5], the investigated temperature range [6] and the method of surface preparation [7,8].

Attempts were made to characterize the oxide growth by way of electrochemical measurements during its formation. In both water and dry environments, the oxide thickening occurs by oxygen migration [9] and a noble metal film could be used to establish a suitable and stable electrical contact at the oxide–gas interface. The potential difference measurements were carried out between this external electrode and the alloy itself. Using Pt film electrodes in steam and oxygen at 500 °C, Urquhart et al. [10] reported the appearance of a potential difference (600–700 mV – Zr negative) as soon as the oxide thickness was larger than the precipitate size. They proposed that the accelerated corrosion is associated to the development of metal-negative potential difference across the film. Different results were obtained by Beie et al. [11] who performed similar experiments in dry

* Corresponding author. Fax: +33-1 69 08 85 52.

E-mail address: jjvermoyal@hotmail.com (J.J. Vermoyal).

[1] Present address: CEA Saclay, DEN/DMN/SEMI/LCMI, Bat. 459, 91191 Gif sur Yvette, France.

0022-3115/01/$ - see front matter
PII: S0022-3115(01)00648-1

oxygen between 300 and 500 °C. Prior to sputtering of the noble metal used as electrode material (Pt), they pre-oxidized the first set of Zy-4 samples for a duration lower than transition time and a second setup to the linear part of the oxidation curve. During oxidation with Pt electrodes, they noticed a potential difference only for the latter set of samples. Concerning the former and even during long heat treatment, no potential difference could be observed, although one would expect this, because the oxide should have grown to a thickness that cannot be bridged by long intermetallics. Noting the contrast with Urquhart results and despite the contradiction with the emf observed for the thicker pre-oxidized specimens, they suggested that high electrostatic fields at the second phase particles could have caused a local oxide breakdown. For β heat-treated Zircaloy-4, Urquhart et al. [10] showed that a 15 nm Pt layer did not modify the oxide film thickness after 24 h in high temperature steam (500 °C, 1500 psi). On the other hand, they reported a drastic increase in corrosion resistance for a standard Zy-4 material Pt-coated (oxide thickness: 3 μm) in comparison to an uncoated specimen (oxide thickness: 250 μm). A catalytic effect was noted by Fiegna and Weisberger [12] on pure Zr coated with a Pt or Ag film (10–30 nm thickness) in water vapor at 450 °C and only with Pt coupling in oxygen. An accelerated corrosion reaction has also been observed at 700 °C in the case of gold-plated pure Van Arkel Zr foils even if a pre-oxidized film is formed before evaporating Au on the specimen [13]. These results show that the coating of a noble metal on the electrochemical reaction sites (ERS) of oxygen reduction (generally assumed to be localized at the oxide–gas interface) is susceptible to modify the oxidation rate if the determining step involves this interfacial process [14], without any diffusion of the noble metal into zirconia which could affect the crystallite growth. In the case of oxygen diffusion control, the only influence of this metallic coupling on the oxide kinetics would be related to the decrease in the ERS number which could be covered by Pt particles.

The purpose of this study is to gain some insight into the mechanism of Zy-4 oxidation, e.g. the kinetic transition to a non-protective oxide film, from information recorded during its growth. In this paper, we report the complementarity of two in situ techniques, the thermogravimetric analyses (TGA) and the electrochemical impedance spectroscopy (EIS), and the results obtained by correlating weight gain measurements and electrical properties of the oxide film.

2. Experimental

Sheets of Zy-4 were provided by Cezus (France). The chemical composition is listed in Table 1 and the size of the second phase intermetallics $Zr(Fe,Cr)_2$ was estimated to be distributed between 150 and 400 nm. Samples of 1–4 cm^2 by 0.1 cm were cut from the same sheet and were decreased and ultrasonically washed successively in acetone, ethanol and pure water for 15 min. In order to avoid a kinetic effect inherent to surface preparation and to study material oxidation narrow industrial use, no specific treatment was applied. Platinum films were deposited by RF sputtering (Plassys) in high purity argon at room temperature. The noble metal is extremely adherent and its thickness was estimated by SEM examinations to be close to 0.5–0.7 μm. For TGA measurements, the entire surface of the sample was coated (2–8 cm^2) and for EIS measurements, only a defined area of 1 cm^2 was used in order to achieve an accurate geometry for the electrochemical cell.

Table 1
Chemical composition of the Zircaloy-4 sheets

Element	Sn	Fe	Cr	C	O	Si
wt%	1.4	0.22	0.108	0.01	0.12	0.0035

EIS and TGA experiments were specifically performed for a duration of 160 h in separated devices but in the same oxidation conditions (500 °C, dry air). Zy-4 samples were set under dry air at 30 °C for 3 h and the temperature was increased to 500 °C at the rate of 99 °C min^{-1}.

The potential developed across the growing oxide was recorded during interruption of impedance measurements using an SI 7157 multimeter (Schlumberger) with a high input impedance (10^{12} Ω).

Five EIS studies were performed on a $Pt/ZrO_2/Zy$-4 cell (Fig. 1). The current collecting was performed through a thin Pt grid on the sputtered electrode and by using a Pt wire (diameter 0.5 mm) spot-welded to the edge of the sheet far from the Pt. At the end of experiments, we checked that no oxide was formed at this welded zone which could result in an additional electrical contribution on impedance diagrams (insulating risk). The identical impedance characteristics of EIS measurements carried out at 500 °C with both the current collectors verify that there is no additional parasitic contribution due to aging of the welding. The electrochemical cell was placed in a furnace where the working temperature was regulated at ±1 °C. Measurements were carried out with a Hewlett–Packard 4192A impedance analyzer within the $5–13 \times 10^6$ Hz frequency range. The low frequency part of diagrams (down to 10^{-3} Hz) was recorded with an autolab frequency response analyzer (Ecochemie). Impedance measurements were performed at rest potential by using a 10–150 mV sinusoidal signal. We checked that both apparatus gave the same response in the common frequency interval. Experimental data were fitted with the equivalent circuit software of Boukamp [15].

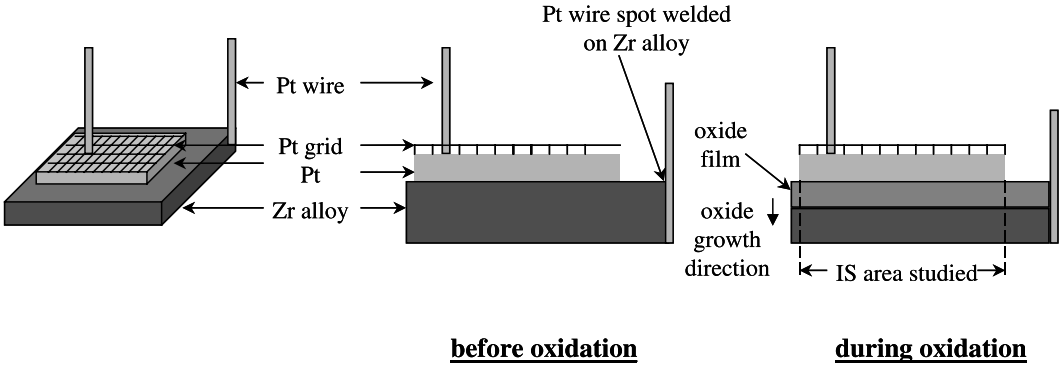

Fig. 1. Scheme of the electrochemical cell.

The oxidation kinetics were characterized by thermogravimetry using a symmetrical Setaram thermobalance (TAG 24 S) with a 1 μg sensitivity. Corrosion test samples for weight gain measurements were supported by a quartz hock in order to avoid any coupling effect with the Pt one classically used for such an experiment.

Thickness and microstructure of oxide films were studied by scanning electron microscopy (SEM). Samples were prepared by standard metallographic techniques, i.e., resin coated, abraded on SiC papers from 240 to 1200 mesh grit and then polished with diamond pastes down to 1 μm.

3. Results

3.1. TGA measurements

Taking 1 μm for 15 mg dm^{-2} [2,16], Fig. 2 shows the variation of the oxide thickness as a function of time for two Pt-coated and two uncoated samples. Similar TGA behavior was recorded for both sets of samples. The most important discrepancy represents 15% of the oxide thickness after 160 h at 500 °C (Table 2) and could be considered as weak in case of a material exhibiting really different oxidation behaviors when coated with a noble metal [10,12–14]. The oxidation curves could be characterized by a cubic rate law followed by a transition to a quasi-linear rate. The rate constant for Zy-4 and Zy-4/Pt was estimated to be close to (0.096 ± 0.025) μm h^{-1} and (0.088 ± 0.050) μm h^{-1}, respectively. These values are slightly higher than those reported in the literature [17]. It is worth noting that these constants depend on different experimental parameters (metallurgical microstructure, surface preparation) as mentioned in Section 1. However, the film thicknesses at the transition were evaluated to be around 2.3–2.5 μm and 2.6–2.7 μm for coated and uncoated specimens, respectively, in a good agreement with previously published data [2].

In the chosen experimental conditions, the Pt film has a columnar structure (Fig. 3) as expected [18]. Accordingly, as previously observed for two Pt-coated Zr alloys coated in the same oxidation conditions [14], oxygen diffusion is likely to occur through the several crystal boundaries. However, the coverage of the Pt film is high enough to identify its apparent area to the geometric one for the external electrode [16].

3.2. EIS results

During the pre-transition stage, the electrical response is firstly composed of the inductive contribution of Pt wires (for frequencies typically higher than 10^6 Hz) and the resistive contribution of the different elements composing the electrochemical cell, meaning a negligible oxide contribution. After several hours, a semi-circle with an increasing amplitude as a function of time was observed in the Nyquist plane (Fig. 4). After the kinetics transition (26–30 h), impedance diagrams are composed of two semi-circles, both characterized by a much larger impedance modulus than during the pre-transition step (Fig. 5).

In a previous paper [16], the electrical properties of oxide films formed on Zr alloys in 360 °C water were studied and the interest of using Cole–Cole diagrams to determine the thickness of oxide layer was evidenced. This kind of representation allows predominantly capacitive systems to be studied owing to the normalization of the admittance by angular frequency ω ($\omega = 2\pi f$). Assuming that the complex impedance $Z^* = Z' - jZ''$, where Z' and Z'' are, respectively, the real and the imaginary parts, is equivalent to series association of a complex capacitance $C^* = C' - jC''$ and a pure resistance R_c, measured at high frequency (i.e., the overall resistance of contacts and connection wires), the expressions of C' and C'' take on the following forms:

$$C' = \frac{1}{\omega} \frac{Z''}{(Z' - R_c)^2 + Z''^2}, \quad (1)$$

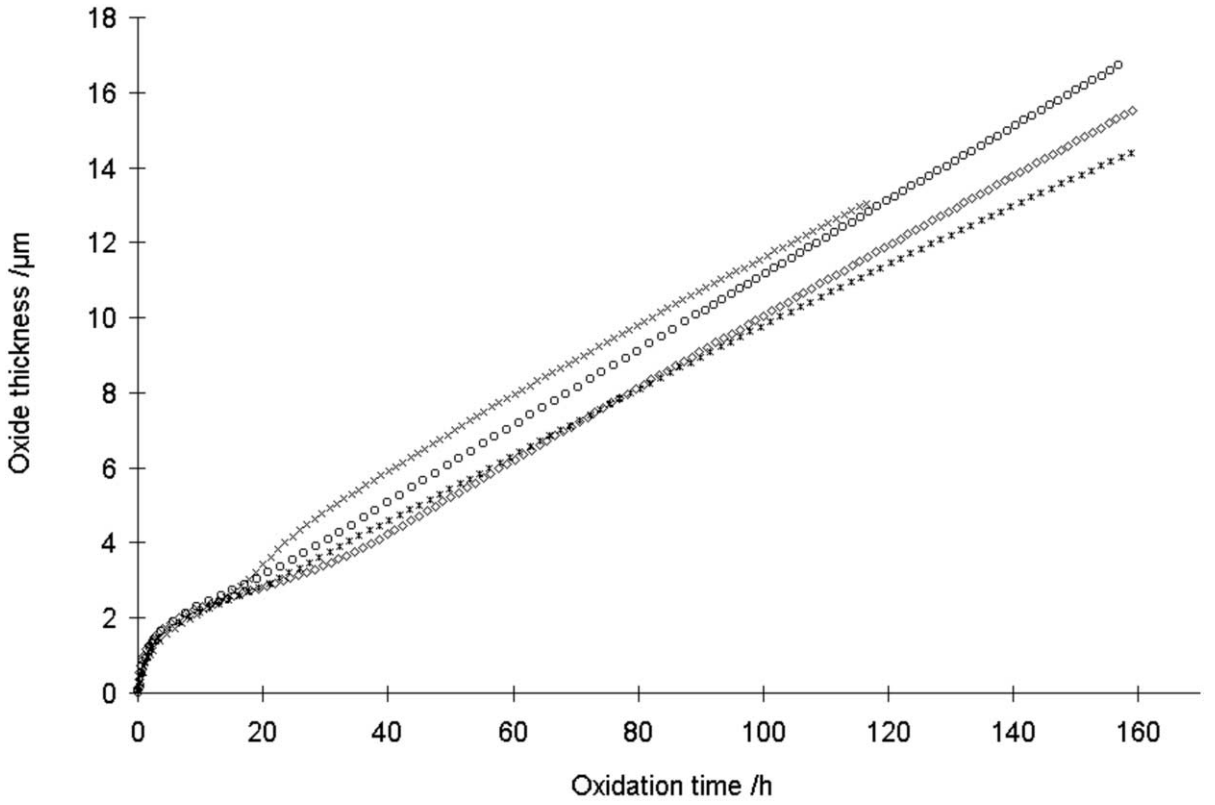

Fig. 2. Oxide thickness versus time for two Pt-coated (Zy-4/Pt: +-×) and two uncoated (Zy-4: ○-◇) samples determined by TGA and oxidation rate (—) versus time for (×) Zy-4/Pt specimen at 500 °C in dry air.

Table 2
Thickness of oxide films formed on coated and uncoated Zy-4 determined by TGA, EIS (room temperature, $\varepsilon = 20$) and SEM (standard deviation is indicated within brackets)

Zr alloys	Oxide thickness/µm		
	TGA	IS	SEM
Coated	14.8 (1.5)	15.3 (0.8)	15.1 (1.1)
Uncoated	15.6 (0.6)	Id	16.8 (1.2)

Id: indeterminable.

$$C'' = \frac{1}{\omega}\frac{Z' - R_c}{(Z' - R_c)^2 + Z''^2}, \tag{2}$$

where R_c is determined by the high frequency intercept of the impedance diagram and the real axis in the Nyquist plane. These values are typically lower than 5 Ω influencing the Cole–Cole diagram shape only for frequencies above 10^6 Hz.

Fig. 6 shows the Cole–Cole diagram recorded after 72 h at 500 °C. The oxide formed on Zy-4 exhibits dielectric dispersion at high frequency (HF) followed by a resistive contribution at lower frequency (note the transition to a more vertical curve) as observed for water corrosion [16]. This HF electrical response could be relevant to the well-known constant phase element (CPE) [19,20], often applied to Zr alloys oxides [21–25] completed in parallel by a real capacitance C_∞. This complementary parameter is needed to account for the real and finite values of the high frequency extrapolation of the linear part of the curve [16].

Such a model could be related to the universal law for the dielectric response proposed by Jonscher [26–28]

$$C^* = C_\infty + \frac{B}{(j\omega)^{1-n}}, \tag{3}$$

where C^* is the complex capacitance of the film ($C^* = C' - jC''$), C_∞ is a pure capacitance related to the oxide thickness and defined as the value of the capacitance C' for infinite frequency. C_∞ is obtained from the high frequency intercept of the linear extrapolation defined by the experimental curve on the real axis in the Cole–Cole plane. B is a constant related to the dielectric dispersion and n is a constant parameter, the dispersion index, characteristic of the constant phase angle between the real axis and the experimental curve.

In order to relate C_∞ to the oxide thickness d, the value of the oxide relative permittivity ε_r at 500 °C is

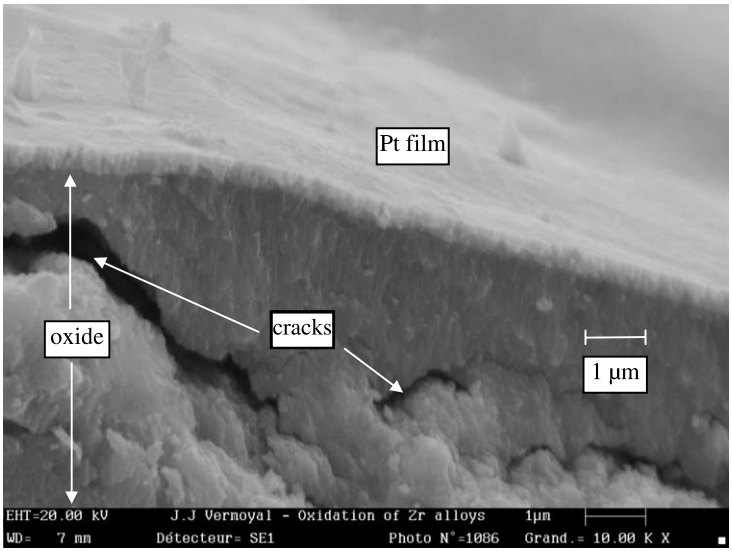

Fig. 3. Fracture cross-section of the external part of an oxide film formed on Zy-4/Pt samples. Specimen was exposed at 500 °C for 160 h.

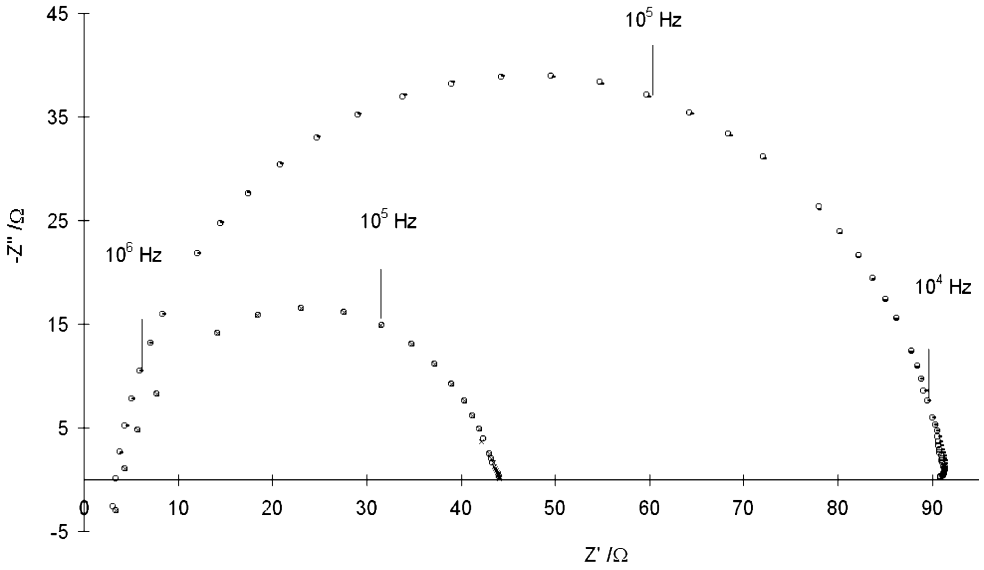

Fig. 4. Experimental Nyquist diagrams recorded in pre-transition period after 2.5 (×) and 8.5 (-) hours and simulated points (○) (see text for further explanations).

required to use the planar capacitance expression $d = \varepsilon_r \varepsilon_0 A / C_\infty$, where ε_0 is the vacuum permittivity and A is the area of the sputtered Pt electrode (assuming the homogeneity of the oxide layer). Therefore, after the last EIS measurements at 500 °C, the temperature was quickly decreased to avoid any further significant oxidation. By assuming that the thickness of the oxide film was not modified during cooling between 500 °C own to room temperature, the following relation could be applied:

$$\varepsilon_{500\ ^\circ C} = \varepsilon_{25\ ^\circ C} \frac{C_{500\ ^\circ C}}{C_{25\ ^\circ C}}, \tag{4}$$

where $C_{25\ ^\circ C}$, $C_{500\ ^\circ C}$, $\varepsilon_{25\ ^\circ C}$ and $\varepsilon_{500\ ^\circ C}$ are the capacitance and the permittivity at, respectively, 25 and 500 °C. Taking $\varepsilon_{25\ ^\circ C} = 22$ [16], a value of $\varepsilon_{500\ ^\circ C} = 24$ was

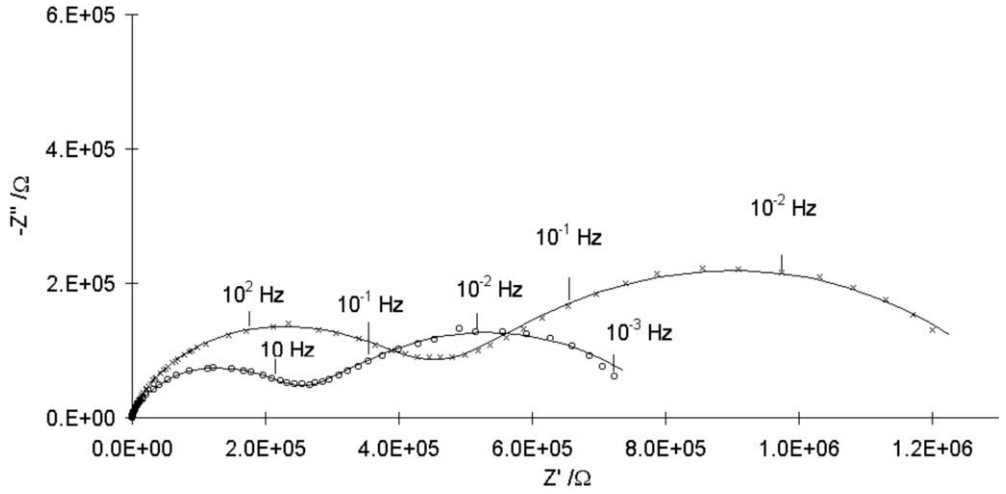

Fig. 5. Nyquist diagrams recorded in post-transition period after 70.5 (○) and 122 (×) h. The continuous line represents the fitted curve calculated from the chosen equivalent circuit (see text for further explanations).

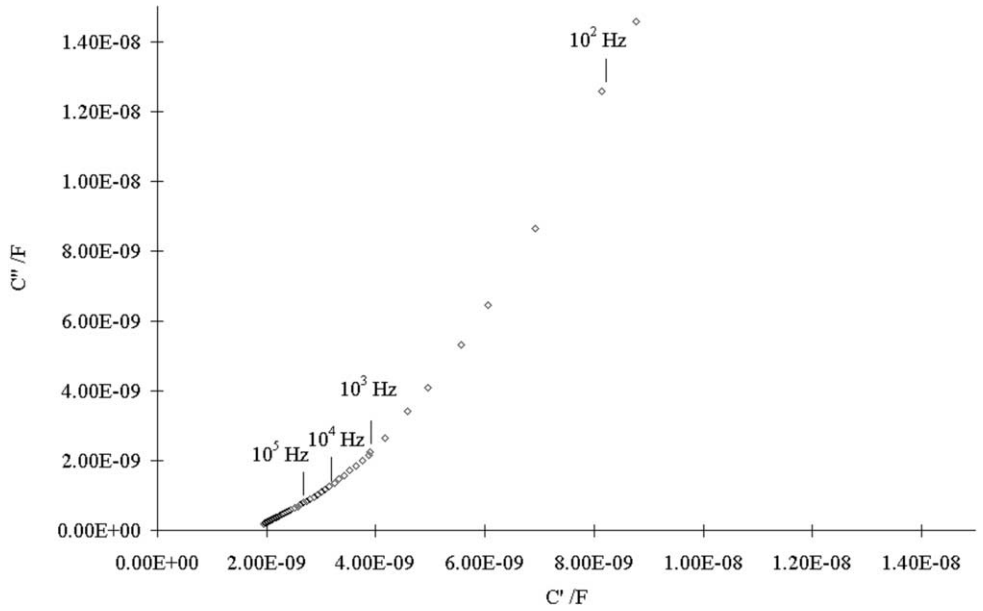

Fig. 6. Cole–Cole diagram obtained after 72 h in dry air at 500 °C.

obtained and this corresponds to a physically reasonable increase of 10% between 25 and 500 °C. A good correlation between oxide thickness values determined by both TGA and EIS was achieved on the basis of C_∞ extrapolation (Fig. 7). Accordingly, any modification of an impedance diagram is relevant to the oxide growth and confers validity to the different assumptions (temperature dependence of ε, Jonscher's relation).

During the pre-transition step, the cell potential is of few millivolts ($\approx$5 mV) and the color of the film (observed at room temperature) is black. After the kinetics transition, the potential increased sharply to 1.2 V (Zr alloy negative) and remained constant until the end of experiments. Concurrently to this electrical modification, the film became light brown.

3.3. SEM observations

Fig. 3 shows the external part of an oxide film formed on a Pt-coated Zy-4 specimen (5 μm under platinum film for a 15 μm total oxide thickness). During the pre-transition, the observed oxide layer appears to be

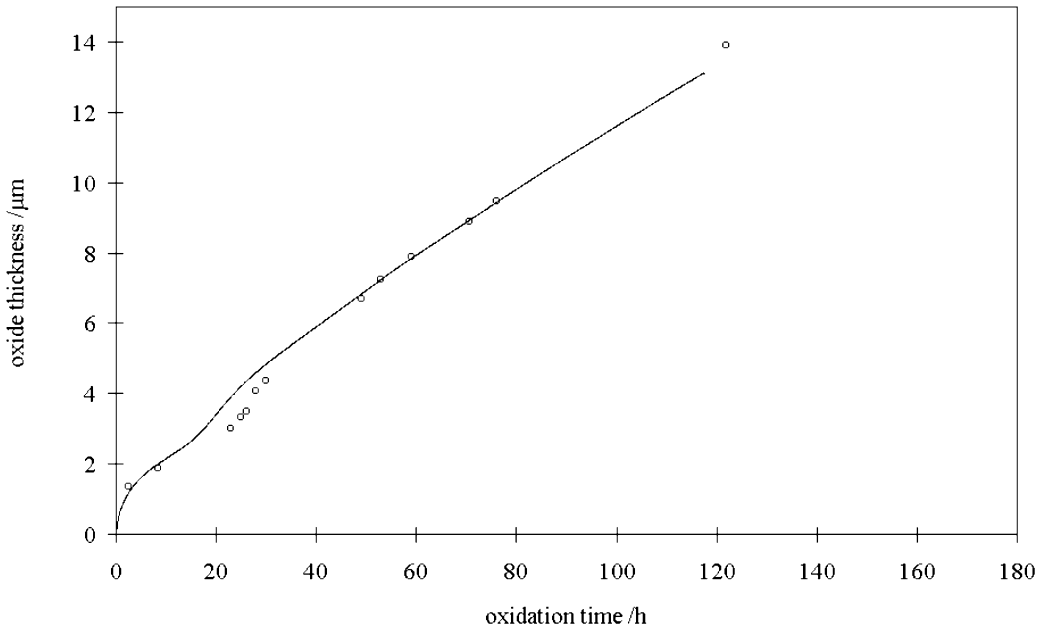

Fig. 7. Variation of the oxide thickness as a function of time determined by TGA (—) and EIS (○).

quite homogeneous and dense. After the kinetics transition, SEM observations reveal the existence of lateral cracks distributed all through the oxide. These cracks have been often related to the kinetic transition and would appear during the relaxation of compressive stress in the oxide [29]. At the end of experiments, the oxide thicknesses determined by SEM examinations are in agreement with the values calculated by TGA and EIS (Table 2).

4. Discussion

4.1. Electrical characterizations

No modification of both the magnitude and frequency distribution of all recorded impedance diagrams was detected by varying the amplitude of the measuring signal between 10 and 150 mV. Accordingly, each semi-circle was related to the oxide response and not to interfacial process (electrochemical reduction or charge transfer processes).

During the pre-transition step (Fig. 4), the single semi-circle could be unambiguously associated to the parallel combination of a capacitor C_{pre} (Jonscher form) and the total resistance of the oxide film, R_{pre} resulting from the ionic and electronic contributions (Fig. 8).

Referring to the literature on the zirconium alloys oxidation [2], the oxide film would degrade to a partially porous one during the post-transition step. The well-defined semi-circle diagrams recorded after the kinetics transition are in agreement with such a microstructure modification of the oxide layer, each layer being characterized by proper conductivity and dielectric constant values. $R_{1,\mathrm{post}}$ and $C_{1,\mathrm{post}}$ represent, respectively, the resistance and the Jonscher capacitance of the HF post-transition contribution and $R_{2,\mathrm{post}}$ and $C_{2,\mathrm{post}}$ account for the layer depicted by the low frequencies (LF) signature. As shown in Fig. 8, both parallel circuits are connected in series. At this stage, it is worth emphasizing that simulation of experimental IS data was performed according to a parallel equivalent circuit (e.g. both electric contributions connected in parallel), as could be assumed in case of localized pathways of highest conductivity within the film. No dispersion parameters could be calculated satisfactorily although resistances were fixed to values easily determined from Nyquist diagrams.

The corresponding fitting results are presented in Figs. 4 and 5. As seen on Nyquist diagrams, the resistance values were easily determined and the discrepancy on calculated electrical parameters was estimated to be lower than 5%. The capacitance values (close to a few nanofarads) are in concordance with the expected dielectric properties of such oxide films. Fig. 9 shows the variation of each layer thickness versus oxidation time calculated from EIS measurements and compared to TGA results (taking $\varepsilon_{500\ ^\circ\mathrm{C}} = 24$). During the first kinetic step, C_{pre} obviously matches C_∞ value in agreement with the single oxide layer model associated to the cubic rate law. As for the post-transition step, the HF thickness obeys an increasing law similar to the time dependence of the total oxide thickness whereas the thickness

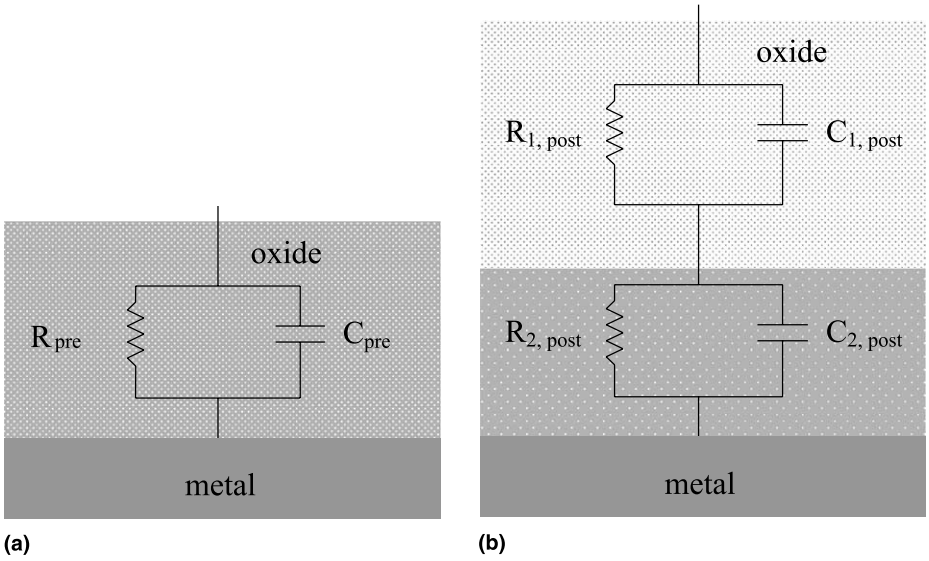

Fig. 8. Equivalent circuits used to fit experimental impedance diagrams for (a) pre-transition and (b) post-transition period.

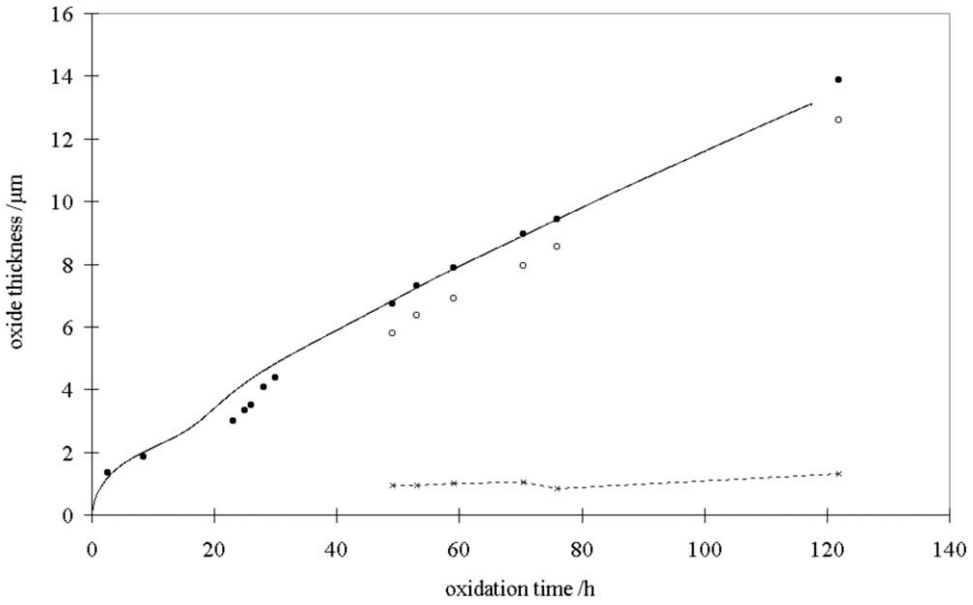

Fig. 9. Variation of the oxide thickness versus time deduced from EIS diagrams for post-transition HF (○) and LF (×) layers. Total oxide thickness determined from EIS (●) and TGA measurements (continuous line).

of the LF signature is nearly constant to 1.1 μm for times up to 120 h (Fig. 9). Finally, one can notice that the sum of both layers' thicknesses perfectly matches the total oxide one estimated from TGA or C_∞ value.

The dispersion index n_{pre} of the pre-transition contribution slightly decreases as a function of time, whereas the $n_{1,post}$ and $n_{2,post}$ parameters are nearly identical and independent of time (about 0.55 ± 0.03) (Fig. 10). Whatever the oxidation period (pre- or post-transition step), the resistances of all contributions are increasing functions of the oxidation time (Fig. 11). However, the increase rate for R_{pre} is drastically higher.

4.2. Oxidation kinetics

4.2.1. Pre-transition

In the pre-transition step, the decreasing rate law was often reported to be closer to a cubic growth kinetic

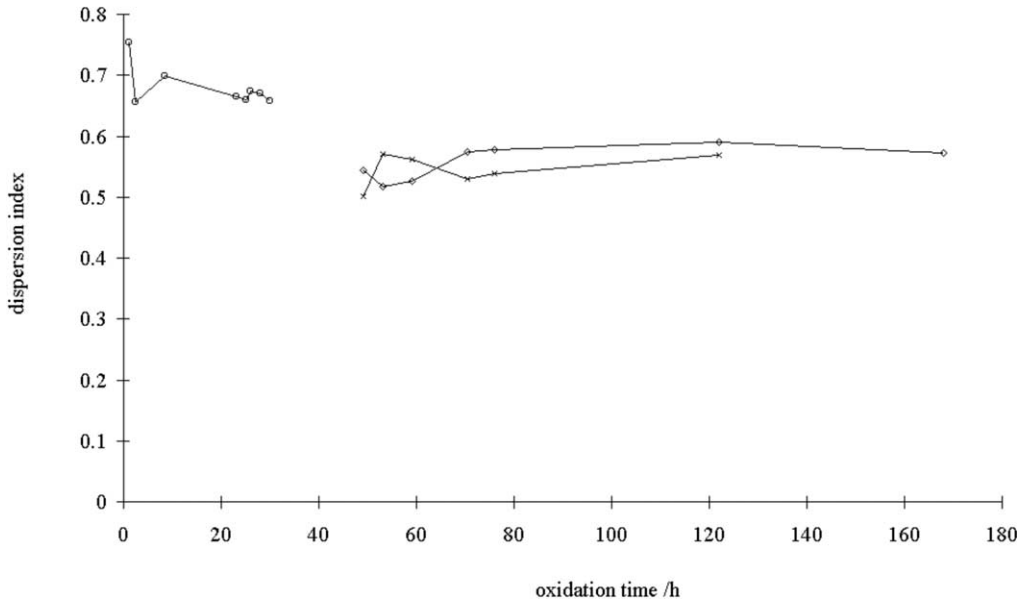

Fig. 10. Variation of the dispersion factors n_{pre} (○), $n_{1,post}$ (◊) and $n_{2,post}$ (×) as a function of time.

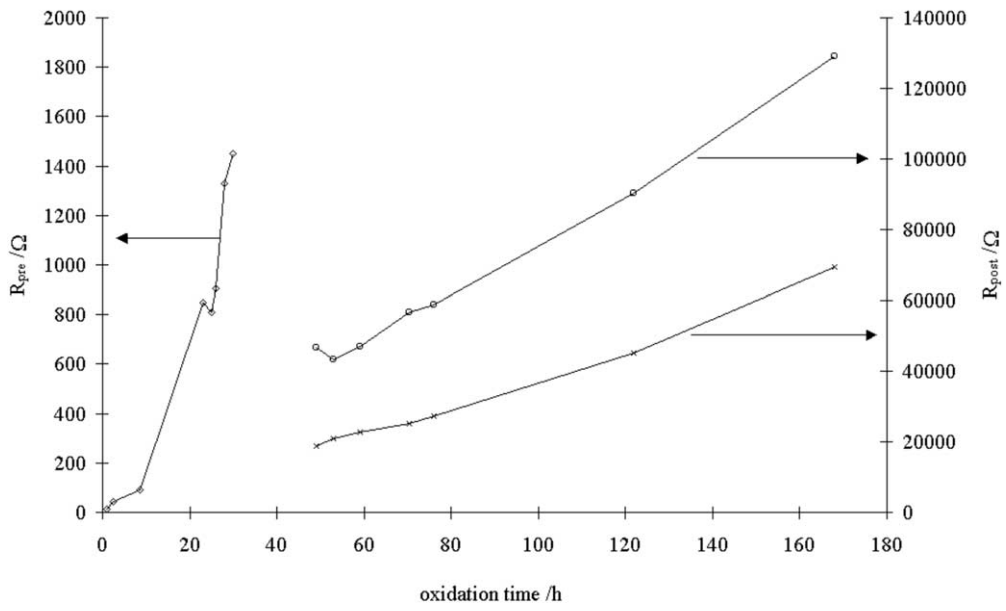

Fig. 11. Variation of the resistances R_{pre} (◊), $R_{1,post}$ (×), and $R_{2,post}$ (○) as a function of time.

curve than the parabolic kinetics predicted by the Wagner–Hauffe theory [29–32] and specially in the case of Zy-4 oxidation at 500 °C in dry air [30]. It is believed that the cubic kinetics arises because the diffusion process controlling oxide growth is not in fact homogeneous in a uniform solid, as required by this theory, but is tightly localized at crystallite boundaries within the oxide [1]. The deviation from the parabola curve was also proposed to be due either to stress growth during the transport of oxygen across a dense oxide layer [2] or to grain size evolution [33]. Noting that the mean crystallite size increases initially as the oxide thickens, Garcia and coworkers [34,35] proposed a qualitative diffusion model considering the dynamic processes of crystallization and recrystallization during oxidation. The modification of the oxygen diffusion coefficient, by decreasing the

number of short-circuit paths within the oxide, is likely to describe the cubic behavior for the pre-transition.

Identical oxidation behaviors of Pt-coated and uncoated Zy-4 samples (Fig. 2) clearly evidence the permeability of the noble metal film to oxygen in agreement with previously published results [10]. The nature of the ERS of oxygen reduction is still under controversy. On the one hand, the ERS are presumed to be the second phase particles $Zr(Fe,Cr)_2$. Evidences show that these intermetallics oxidizing after the Zr matrix are localized regions of high conductivity [36,37]. Although they are generally thought to give rise to short-circuits [22,38], the pathway of the electrons through the oxide film has not been completely identified. On the other hand, the preferred sites for cathodic reduction were shown to be most readily scratches and cracks and not the second phase particles in thin oxides [22].

In case of Pt-coated sheets, the ERS (whatever their location) do not seem to be modified by the noble metal film and the oxide growth does not depend on this parameter. Taking into account that IS investigations reveal only one electrical contribution and that no interface process is rate-determining, the cubic kinetics is compatible with the accepted classical assumption of oxygen diffusion through a dense oxide film.

Both low emf values and black color of the oxide suggest a high level of non-stoichiometry of the oxide and a main electronic conduction process [1,10]. The electronic contribution could be regarded as resulting in either of the intrinsic properties of the oxide or mostly of the precipitates' contribution. As a complement, the increased resistive properties of the film during annealing indicate that no short-circuits or charge percolation process occurred. Accordingly, without any microstructure modification, the electrical signature was ascribed to a single dense oxide. The time variations of the oxide resistance do not obey the cubic kinetic law of oxidation in contrast to the reciprocal capacitance. Thus, the resistance increase during the pre-transition step is not only related to a simple growth geometric effect, but could be associated to:

- a modification of the oxide stoichiometry,
- a progressive oxidation of the second phase particles,
- a modification of the ionic and electronic transport numbers during the oxide growth.

4.2.2. Post-transition

As observed previously by Urquhart et al. [10], an increase of the cell potential can be related to the kinetics transition. For the post-transition step, the significant variations of both color and impedance modulus of the oxide can be viewed as indicative of an increasing stoichiometry of the film. The slight different rate constant values between coated and uncoated specimens were assumed to result from the imposition of an equipotential on the oxide surface due to the high conductivity of the sputtered platinum [10]. Nevertheless, no interpretation has actually been established. At the transition point, the oxide layer was often seen to lose its protective character [2], resulting in a more direct access of corrosion environment close to or at the metal surface. These changes would be correlated to the large access of oxygen through the porosity of the degraded layer and to the resulting decrease in oxygen vacancies and electron concentration.

By assuming a partial degradation of the oxide into a porous layer (HF electrical signature) and a barrier layer (LF signature) [16], IS measurements indicate a time independent thickness of the dense part during the quasi-linear part of the kinetics. This observation agrees with an oxygen diffusion through a film of constant thickness. The thickness of the barrier layer (1.1 ± 0.15 μm) is contained between the values determined by optical [29] and IS [39] investigations of oxide layers formed in high temperature water (2 μm) and those estimated by IS measurements on different Zr-based materials in a 400 °C steam (0.85–1.2 μm) [40]. Noting that IS data give an average indication in relation to the whole electrode area investigated, the apparent constant thickness of the dense layer might result from a vast number of localized degradations and so, to a multitude of repeated cycles of cube-root kinetics [29]. Accordingly, the observed linear post-transition kinetics would be the average corrosion rate.

During the constant rate oxidation, both the resistances of porous ($R_{1,\mathrm{post}}$) and dense layers ($R_{2,\mathrm{post}}$) increased as a function of time. The product $R_{1,\mathrm{post}}C_{1,\mathrm{post}}$ which represents the resistivity of the layer (for a constant dielectric permittivity) does not depend on time. This result suggests a simple geometric growth of the porous layer. This observation is supported by the constant value of the potential which could be regarded as the IR drop through the outer porous layer since Pt coating is supposed to lose the contact with the ERS when the oxide becomes porous.

As for the dense layer in pre-transition, the resistance of the barrier layer (LF) does not obey the same law as the kinetic curve. $R_{2,\mathrm{post}}$ increases as a function of time indicating a modification of the dense layer resistivity since its thickness is constant.

The electrical properties of the protective layer were observed to be quite different in pre- and post-transition owing to the modification of the dispersion index n. By EIS characterization in liquid medium at room temperature, Barberis and coworkers [41,42] also reported a considerable evolution of the dispersion index of the inner layer relative to Zy-4 oxide formed in a 400 °C steam. Although the physical meaning of the dispersive parameter is still to be identified, the degradation of the oxide resistance to corrosion could be correlated to the alteration of the electrical 'barrier character' of the pre-transition film. In the same way, the final values of n are

close to those determined in this study (0.55). In connection to kinetics properties, it is worth noting that these values could be related to a diffusion mechanism (0.5).

As shown in Fig. 9, the two electrical signatures appear after the kinetics transition. The modification of the oxide film in two layers could then be the consequence of the transition rather than the origin. On the other hand, the electrical difference properties of both layers could not quite be electrically differentiated after the kinetics acceleration to be immediately observable. The view of each signature would be delayed to a longer time so it is not possible to conclude about the mechanism of transition initiation.

5. Conclusion

The Pt independent behavior of Zircaloy-4 is associated to a rapid transition from a cubic to a linear kinetic law. This behavior agrees with an oxygen diffusion rate determining step. Electrochemical measurements show the initially high non-stoichiometry of a single barrier layer in which degradation into a partially porous oxide at the kinetic transition was proposed. In post-transition, impedance spectra are characterized by two contributions associated to the electrical responses of a barrier layer and a porous one. The linear corrosion rate was interpreted as the diffusion limited transport through the inner layer with an average constant thickness of about 1 μm. Further work will have to explain the relation between electrical and mechanical properties in order to shed some light on the progressive and constant degradation of the porous part of the oxide.

Acknowledgements

The authors gratefully acknowledge Cezus (France) for supplying Zircaloy-4 specimens and Framatome for funding this work, and Sylvie Bragard for valuable discussions.

References

[1] B. Cox, J.P. Pemsler, J. Nucl. Mater. 28 (1968) 73.
[2] Waterside Corrosion of Zirconium Alloys in Nuclear Power Plants, IAEA-TECDOC-996, IAEA, Vienna, 1998.
[3] R. Hussey, W. Smeltzer, J. Electrochem. Soc. 111 (1964) 564.
[4] H. Porte, J. Schnizlein, R. Vogel, D. Fischer, J. Electrochem. Soc. 107 (1960) 506.
[5] C.M. Eucken, in: Proceedings of the Eighth Symposium of the Zirconium in the Nuclear Industry, ASTM-STP 1023, American Society for Testing and Materials, Philadelphia, PA, 1989, p. 113.
[6] P. Kofstad, Acta Chem. Scand. 12 (1958) 701.
[7] E.A. Gulbransen, K.F. Andrew, J. Met. 9 (1957) 394.
[8] J. Belle, M.W. Mallett, J. Electrochem. Soc. 101 (1954) 339.
[9] A. Grandjean, Y. Serruys, J. Nucl. Mater. 273 (1999) 11.
[10] A. Urquhart, D. Vermilyea, W. Rocco, J. Electrochem. Soc. 125 (1978) 199.
[11] H.J. Beie, A. Mitwalsky, F. Garzarolli, H. Ruhmnann, H.S. Sell, in: Proceedings of the 10th Symposium of the Zirconium in the Nuclear Industry, ASTM-STP 1245, American Society for Testing and Materials, Philadelphia, PA, 1994, p. 615.
[12] A. Fiegna, P. Weisberger, J. Electrochem. Soc. 115 (1968) 369.
[13] D. Bradhurst, J. Draley, J. Van Drunen, J. Electrochem. Soc. 112 (1965) 1171.
[14] J.J. Vermoyal, A.L. Sauvet, L. Dessemond, A. Frichet, Poster session, 8th International Symposium on Passivity of Metals and Semiconductors, Jasper, Alberta, Canada, 9–14 May 1999, to be published.
[15] B. Boukamp, Solid State Ionics 20 (1986) 31.
[16] J.J. Vermoyal, A. Frichet, L. Dessemond, A. Hammou, Electrochim. Acta 45 (1999) 1039.
[17] M. Suzuki, S. Kawasaki, J. Nucl. Mater. 140 (1986) 32.
[18] A. Richard, A.N. Durand, La pratique du Vide et les Dépôts en Couches Minces (in Fr.), Ed. In Fine, Paris, 1995.
[19] K. Jüttner, W.J. Lorenz, M.W. Kendig, F. Mansfeld, J. Electrochem. Soc. 135 (1989) 332.
[20] K. Jüttner, Electrochim. Acta 35 (1990) 1501.
[21] O. Gebhardt, J. Nucl. Mater. 203 (1993) 17.
[22] O. Gebhardt, A. Hermann, Electrochim. Acta 41 (1996) 1181.
[23] B. Cox, F. Gauducheau, Y.M. Wong, J. Nucl. Mater. 189 (1992) 362.
[24] N. Ramasubramanian, J. Nucl. Mater. 55 (1975) 134.
[25] R. Kruger, R. Adamson, S. Brenner, J. Nucl. Mater. 189 (1992) 318.
[26] A.K. Jonscher, Dielectric Relaxation in Solids, Chelsea, London, 1983.
[27] A.K. Jonscher, J. Mater. Sci. 16 (1981) 2037.
[28] A.K. Jonscher, Nature 253 (1975) 717.
[29] J. Bryner, J. Nucl. Mater. 226 (1979) 34.
[30] J.K. Dawson, G, Long, W. Seddon, J.F. White, J. Nucl. Mater. 25 (1968) 179.
[31] J. Nakamura, M. Hashimoto, T. Otomo, S. Kawasaki, J. Nucl. Mater. 200 (1993) 256.
[32] A.J.G. Maroto, R. Bordoni, M. Villegas, A.M. Olmedo, M.A. Blesa, A. Iglesias, P. Koenig, J. Nucl. Mater. 229 (1996) 79.
[33] G. Sabol, S. Dalgaard, J. Electrochem. Soc. 122 (1975) 316.
[34] E.A. Garcia, J. Nucl. Mater. 224 (1995) 299.
[35] E.A. Garcia, J. Kovacs, J. Nucl. Mater. 210 (1994) 78.
[36] P.J. Shirvington, J. Nucl. Mater. 37 (1970) 177.
[37] P.J. Shirvington, B. Cox, J. Nucl. Mater. 35 (1970) 211.
[38] B. Cox, Y.M. Wong, J. Nucl. Mater. 218 (1995) 324.
[39] H. Göhr, J. Schaller, H. Ruhman, F. Garzarolli, in: Proceedings of the 11th Symposium of the Zirconium in the Nuclear Industry, ASTM-STP 1295, American Society for Testing and Materials, Philadelphia, PA, 1996, p. 181.

[40] G. Wilmark, P. Rudling, B. Lethinen, B. Hutchinson, A. Oscarsson, E. Ahlberg, in: Proceedings of the 11th Symposium of the Zirconium in the Nuclear Industry, ASTM-STP 1295, American Society for Testing and Materials, Philadelphia, PA, 1996, p. 55.
[41] P. Barberis, A. Frichet, J. Nucl. Mater. 273 (1999) 182.
[42] P. Bossis, G. Lelièvre, P. Barberis, X. Iltis, F. Lefebvre, in: Proceedings of the 12th Symposium of the Zirconium in the Nuclear Industry, ASTM-STP 1354, American Society for Testing and Materials, Philadelphia, PA, 2000, p. 918.